Research Article Vol. 57, No. 24 / 20 August 2018 / Applied Optics 7055

applied optics

High single-fundamental-mode power VCSEL integrated with alternating aluminum content micro-lens

Youwen Huang,[1] Xing Zhang,[1,*] Jianwei Zhang,[1] Werner Hofmann,[2] Yongqiang Ning,[1] and Lijun Wang[1]

[1]Changchun Institute of Optics, Fine Mechanics and Physics, Chinese Academy of Sciences, Changchun 130033, China
[2]School of Solid State Physics, Technical University of Berlin, Berlin 10623, Germany
*Corresponding author: zhangx@ciomp.ac.cn

Received 3 April 2018; revised 28 June 2018; accepted 3 July 2018; posted 25 July 2018 (Doc. ID 327573); published 20 August 2018

The patterned top-emitting vertical-cavity surface-emitting laser (VCSEL) with a fixed diameter etching window was etched in hydrobromic acid solution with anisotropic etching. An all-semiconductor micro-lens that consisted of alternating aluminum content was directly formed on the output window. The etched curved surface with designed curvature radius makes the mirror loss located at the convex region differ from the edge region. Higher-order modes experience larger mirror loss and are therefore filtered out. The VCSEL with the designed micro-lens reaches a 3.14 mW single-mode power with side-mode suppression ratio >25 dB, which is over 50 times higher than the 0.06 mW single-mode power of the reference VCSEL.

OCIS codes: (250.5960) Semiconductor lasers; (250.7260) Vertical cavity surface emitting lasers; (140.3300) Laser beam shaping; (140.3295) Laser beam characterization.

https://doi.org/10.1364/AO.57.007055

1. INTRODUCTION

The inherent advantages, longitudinal single-mode emission, circular beam shape, ultra-low threshold currents and power consumption, make vertical-cavity surface-emitting lasers (VCSELs) the desired ideal light source in the areas of fiber-optic communication and optical interconnects, in which the single-mode emitting VCSEL is of crucial importance. However, the multi-transverse-mode operation and lower beam quality of an unprocessed VCSEL raise the cost for beam shaping, packaging, and optical fiber coupling. Many methods and technologies had been proposed to obtain single-transverse-mode VCSEL. An invariable principle buried behind them is the considerable difference in mirror loss suffered by the fundamental mode and high-order mode. Existing methods of VCSEL mode control, such as shallowed surface relief, require redesign of the epi-wafer structure and precise etching depth control [1], and buried heterostructures, restricted by limited availability of materials suitable for lattice-matched regrowth and problems of the quality of the regrowth interface [2,3]. Furthermore, the proton-implanted VCSEL presents unstable, current-dependent beam characteristics [4,5] and photonics crystal defects introducing larger optical loss and electrical resistance [6,7], and are accompanied with sophisticated fabrication process, accurate control, and expensive equipment.

Micro-lenses monolithically integrated on the VCSEL output window is a potential method to control the mode profile. That has been numerically investigated in [8]. Numerous methods to fabricate micro-lenses have been applied, which can be classified based on the materials forming the micro-lens. On the one hand, the photoresist and polymer micro-lenses can be fabricated by thermal reflow technology or direct laser write technology and reactive ion etching (RIE)/inductively coupled plasma (ICP) etching [9–11]. However, the organic materials cannot withstand the high temperatures or organic solvents, which greatly limit the practicability of this method. Micro-lenses fabricated by sputtered dielectric films and ICP/RIE etching can achieve improved VCSEL output performance [12,13]. Nevertheless, integrating such a micro-lens into a VCSEL structure requires sophisticated sputtering and dry-etching equipment with precise process control.

In this paper, we present a VCSEL integrated with micro-lens formed by alternating aluminum content material. The transfer matrix method was applied to calculate the radial variation of reflectivity and mirror loss changing with radial etching depth. Eventually, a slow etching depth varying curved micro-lens was designed. The diffusion-limited wet chemical etching was applied to etch the top surface of the top-emitting VCSEL and form a micro-lens. Varied mirror loss was

introduced to filter out the high-order modes emitted from the conventional VCSEL.

2. DEVICE DESIGN AND FABRICATION

The VCSEL wafer was grown on the (100) GaAs substrate by AIXTRON 200-4 metal organic chemical vapor deposition and designed for emitting at a wavelength of 850 nm. Three GaAs quantum wells separated by a AlGaAs barrier constituted the active layer. A 30 nm thick high aluminum content layer was inserted to be oxidized about 6 min at 420°C under nitrogen gas bubbled through water at 90°C to form a current aperture with a diameter of 5 μm. The *p*-type distributed Bragg reflector (DBR) was stacked up by 23 pairs of alternative quarter-wavelength thick C-doping $Al_{0.12}Ga_{0.88}As/Al_{0.9}Ga_{0.1}As$ layers. The bottom DBR consisted of 34.5 pairs of Si-doping $Al_{0.12}Ga_{0.88}As/Al_{0.9}Ga_{0.1}As$ layers.

What we expected is the variation in etching depth on the output window to introduce considerable mirror loss for fundamental- and higher-order modes. To our knowledge, we can take full advantage of the anisotropic etching of Br_2 molecules dissolved in solution to etch the output window of the top-emitting VCSEL. Thus, the radial variation in the etching rate at the edge and the center region of the circular hole enabled an aspheric profile on the surface of emitting window to be formed. The vertex region of the micro-lens experiences much less mirror loss so that the fundamental mode located at the center of mesa acquires the minimum threshold gain to be lased first. The edge region of the micro-lens suffers from considerable cavity mirror loss. The most of the power of the high-order mode tending to the edge of the micro-lens experiences larger threshold gain to be suppressed. Figure 1 shows the cross section of the designed monolithic integrated micro-lens VCSEL.

We had divided the cap layer and p-DBR into large numbers of slices. The transfer matrix method was applied to calculate the reflectivity of the p-DBR with sample etch depth. The result is shown in Fig. 2(a). The wavy reflectivity presents periodic variation, and the center corresponds to the maximum of reflectivity and the center of the mesa. Over the entire output surface, the reflectivity with the same etching depth forms a

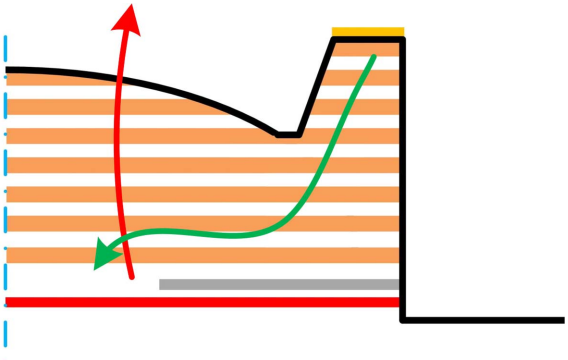

Fig. 1. Half of the schematic cross section of the designed micro-lens formed by etching the p-side light-emitting window into the p-DBR. The current flow injects throughout the ring-shaped contact and is signed by the green arrow, and the red arrow represents the light emitting.

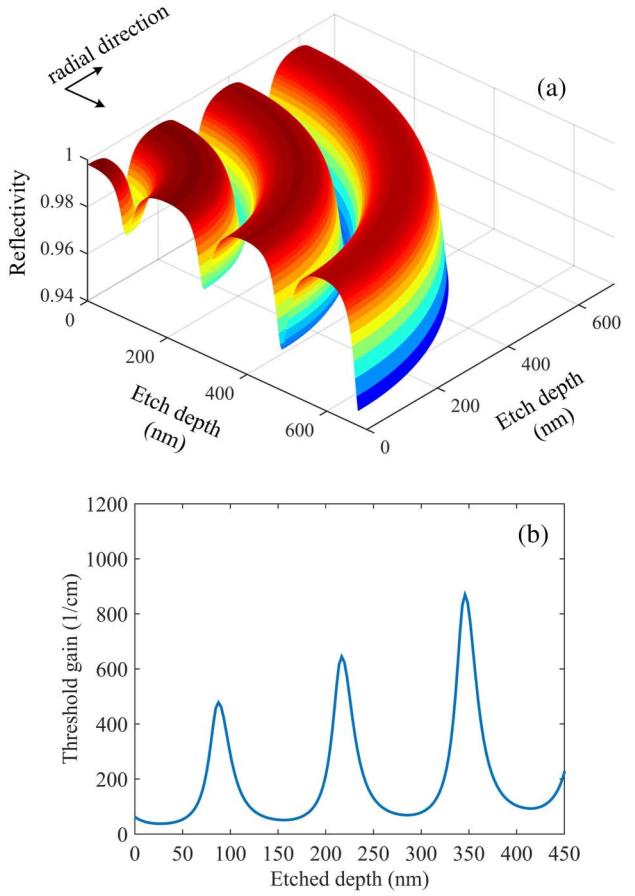

Fig. 2. (a) Radial reflectivity of one fourth remaining p-side structure versus the longitudinal sampling etching depth. (b) Effect of the etched depth on the threshold gain of the VCSEL. (Optical confinement factor is 0.021, and the cavity-length of the VCSEL is a wavelength.)

circular ring. At some special sampling etching depths, the reflectivity varies from the maximum to the minimum rapidly. Moreover, we also calculated the threshold gain of the VCSEL with the sample etch depth, and the result was shown in Fig. 2(b). On the contrary, the sampling depths with minimum threshold gain correspond to the maximum reflectivity. Therefore, the considerable difference in threshold gain and reflectivity enables modes to be distinguished.

A series of numerical simulations were carried out for demonstrating the capacity of the micro-lens for mode controlling. A photonic micro-cavity finite-difference time-domain model was built to simulate the optical field distribution inside of the cavity of the micro-lens integrated VCSEL. The device structure model was kept the same as what is shown in Fig. 1. In our model, the actual multi-layer micro-lens was displaced by a homogeneous GaAs aspherical cap to reduce the difficulty in modeling. The diameter of 9 μm and the aspherical constant of 2 were defined by the atomic force microscope (AFM) measurement result of the pre-processed etched micro-lens sample [14]. The active region was set to be with gain medium. In the process of simulation, we fixed the diameter and changed the heights of the micro-lens to

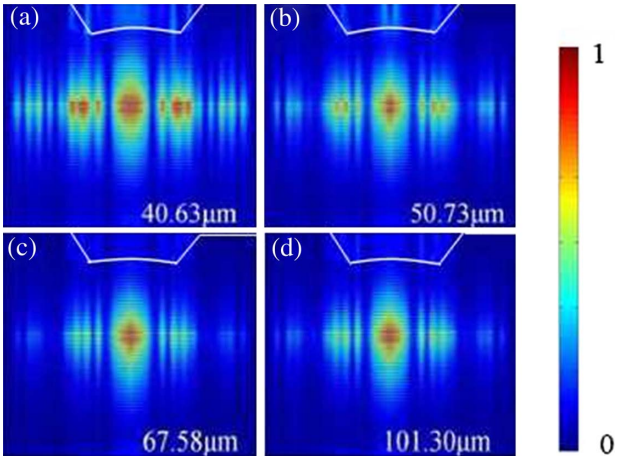

Fig. 3. Simulated internal optical field distribution of the micro-lens integrated VCSEL. The values of curvature radius R_c are (a) 40.63 μm (height 250 nm), (b) 50.73 μm (height 200 nm), (c) 67.58 μm (height 150 nm), and (d) 101.30 μm (height 100 nm).

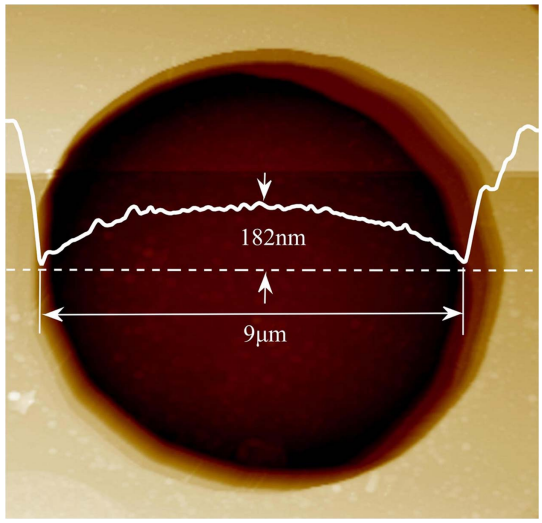

Fig. 4. Surface profile measured by atomic force microscopy (AFM).

obtain a different curvature radius micro-lens. A dipole source located inside of the cavity was expected to excite all the modes supported by the device. The wavelength was set to be 850 nm. The anti-symmetric and symmetric boundary conditions were applied to diminish the calculation amount and lower the memory consumption of the computer. The transverse modes analysis was performed through the photonic micro-cavity model. The variation mirror loss of the cavity mode introduced by the nonplanar aspheric surface can distinguish the transverse modes in the cavity. The vertex region of the micro-lens experienced much less mirror loss and the beneath area in the active region suffered from much less gain loss. The simulation results are shown in Fig. 3. When R_c is larger than 50.7 μm the **E**-field concentrates in the center of the cavity, which means that the fundamental mode operation can be achieved. Higher-order transverse modes will be excited when R_c decreases down to 40.6 μm. A micro-lens with curvature radius less than 40.63 μm or larger than 50.7 μm is necessary for prompting the fundamental mode to dominate the optical field in the cavity of the micro-lens VCSEL. Therefore, the stable and precise etching process is essential for forming of the micro-lens VCSEL.

In this paper, the fabrication process of the VCSEL with an all-semiconductor monolithic integrated micro-lens added an additional lithography and a wet etching instead of sophisticated and unstable ICP/RIE etch and thermal reflow. After p-contact metal deposition, we lifted off the metal and the remaining photoresist covering the light-emitting window. A lithography process was carried out to fabricate the wet-etching mask, which was defined by the remaining unexposed circular-hole photoresist membrane. Then, the patterned wafer was immersed in the wet chemical etchant, a mixture of H_2O_2, HBr, CH_3OH, and H_2O at the ratio of 1∶1∶1∶10 in volume [15–17]. The methanol was added to dissolve the produced Br_2 molecules and make it adhere to the etching surface better for a smoother etching surface. The etching rate was slowed down by putting the beaker with etchant in the ice water and maintaining it for some time to decrease the temperature of the mixture liquid. The etch depth was controlled by etch time. The AFM technique was employed to characterize the surface profile of the micro-lens. The measurement result is shown in Fig. 4. The curvature radius of R_c and focus length can be calculated according to the height of 182 nm and the diameter of 9.00 μm. They are 55.63 μm and $55.63/(n-1)$ μm, respectively [14].

3. RESULTS AND DISCUSSION

The output characteristics of two types of VCSELs at room temperature are shown in Fig. 5. The threshold current and the maximum output power of the conventional VCSEL are found to be 0.9 mA and 5.37 mW. However, the single-mode output power at threshold is only 0.06 mW. The VCSEL with a micro-lens has a threshold current of 0.8 mA and emits maximum output power of 6.18 mW. When the current injection level is below 4 mA, the VCSEL emits a single transverse mode and the maximum single-mode output power is 3.14 mW at 4 mA.

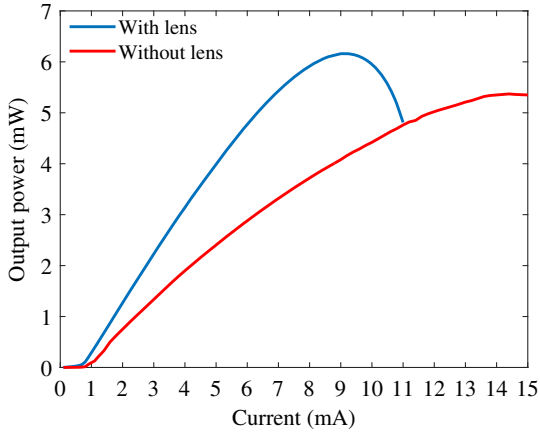

Fig. 5. $P-I$ characteristics of the conventional VCSEL and micro-lens integrated VCSEL.

The maximum output power of the structured VCSEL is larger than the one of the conventional VCSEL. The output window of the structured VCSEL had been etched to form a nonplanar aspheric surface. The reflectivity of the etched upper DBRs presents periodic variation over the entire output window. A reduction of upper mirror reflectivity results in an increase of the maximum output power of the processed VCSEL. On the other hand, the threshold current of VCSEL with a micro-lens is less than the conventional one. We explain this behavior with better focusing of the spherical emission window and the feedback light overlapping with the quantum-well active layer. As well, the total accumulative feedback light that came from the micro-lens surface strengthens the field strength in the quantum-well active layer. All the three pre-mentioned causes may lead to the steeper slope efficiency and smaller threshold current of the micro-lens VCSEL. We explain the lens-VCSEL with much quicker thermal rollover with remaining narrowed current injection path after the etching process. The increased resistance caused by the narrowed current path produces more heat when the lens-VCSEL is in forward current bias.

Figures 6(a)–6(d) show the lasing spectra of the micro-lens integrated VCSEL at a current injection of $I = 1$–4 mA, and Figs. 6(e)–6(h) display the spectra of the conventional VCSEL at threshold and $I = 1$–4 mA. All spectra were taken with a resolution of 0.02 nm at room temperature. The conventional VCSEL emits a single-peak spectrum at threshold of 0.9 mA, which is shown in Fig. 6(e). Afterwards, the multi-peak spectra of the conventional VCSEL rise above the threshold current. That indicates the existence of multi-transverse mode. Conversely, the spectra in Figs. 6(a) and 6(b) show a single peak at −36.2 dBm and −41.5 dBm, respectively. The lateral side mode appears from the current injection of 3 mA. The intensity of the fourth mode rises speedily with the increasing of the injection current. However, the fundamental mode with side-mode suppression ratios of 32.04 and 25.91 dB dominates the spectra in Figs. 6(c) and 6(d). Moreover, the cavity mode of the VCSELs with micro-lens has an emission more blue compared to the reference VCSEL. Therefore, the micro-lens integrated VCSEL can maintain single-mode operation when the current injects below 4 mA.

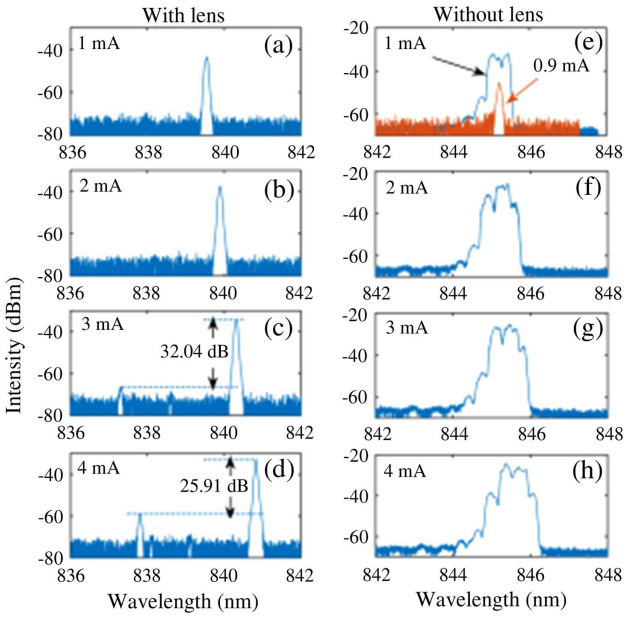

Fig. 6. Spectra of the micro-lens integrated VCSEL (left column) at a current injection of $I = 1$–4 mA; spectra of the conventional VCSEL (right column) at threshold and $I = 1$–4 mA.

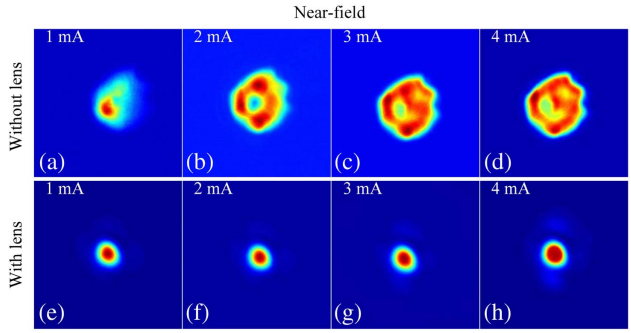

Fig. 7. Near-field patterns of the conventional VCSEL at (a) $I = 1$ mA, (b) $I = 2$ mA, (c) $I = 3$ mA, and (d) $I = 4$ mA. Near-field patterns of the micro-lens integrated VCSEL at (e) $I = 1$ mA, (f) $I = 2$ mA, (g) $I = 3$ mA, and (h) $I = 4$ mA.

We measured the near-field patterns of two types of VCSELs at different current injection levels. Figures 7(a)–7(d) show the near-field patterns of the conventional VCSEL at injection currents of $I = 1$, 2, 3, and 4 mA. The multi-lobe near-field patterns were observed at all current injection levels, which indicates that the conventional VCSEL emits multi-transverse modes. The multi-lobe patterns of the conventional VCSEL coincide with the multi-extremum spectra shown in Figs. 6(e)–6(h). Simultaneously, the near-field patterns of the VCSEL with micro-lens were measured under the same condition and the results are shown in Figs. 7(a)–7(d). The near-field patterns in Figs. 7(e)–7(h) show a single lobe, which

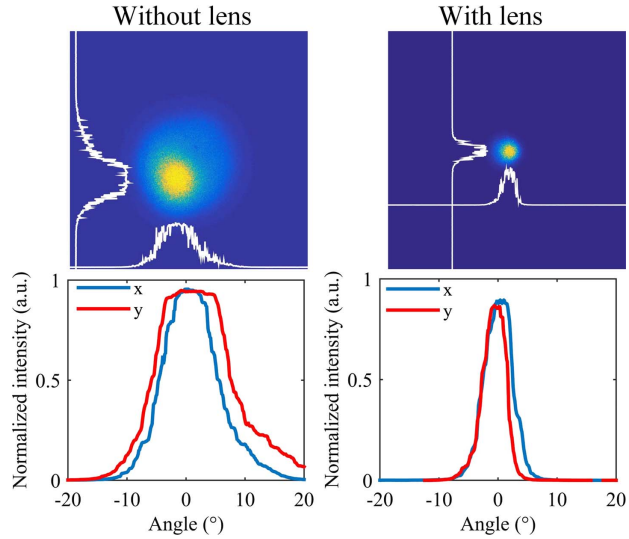

Fig. 8. Far-field patterns and intensity profiles along the x axis and y axis of the conventional VCSEL (left) and the micro-lens integrated VCSEL (right) at $I = 4$ mA.

is consistent with the spectra with a dominated lasing mode in Figs. 6(a)–6(d). The micro-lens etched into the p-DBR of the VCSEL is successful in filtering out more high-order modes emitted from the conventional VCSEL.

The far-field profiles of two types of VCSELs with current injection $I = 4$ mA were measured and characterized. The results and their intensity profiles along the x axis and y axis are shown in Fig. 8. The beam sizes of the VCSEL with micro-lens are much smaller than those of the unprocessed VCSELs. That indicates that the micro-lens integrated onto the output window compressing the divergence angles effectively. The feedback light from the vertex area of the alternating aluminum content micro-lens was stronger than that from the edge of the micro-lens. The field strength of the quantum well in the active layer of the aperture center improved and spatially concentrated near this aperture center. Consequently, the far-field patterns of the VCSEL with micro-lens were compressed almost twice.

4. CONCLUSION

The proposed micro-lens integrated VCSEL was fabricated by etching the p-side output window onto the p-DBR. The anisotropic etching of dibromine resulted in spatial variation in etch rate over the entire output window and formation of the micro-lens. A large difference in mirror loss along the radial direction of the output window was introduced. High-order modes located at the marginal area of the micro-lens suffered greater loss than the fundamental mode situated in the vertex region of the micro-lens experienced. Therefore, the high-order modes can be filtered out. In this paper, we eventually fabricated the VCSEL integrated with the micro-lens. In contrast to the reference VCSEL, over 50 times' enhanced single-mode power and nearly twice compressed divergence angle were obtained from the micro-lens VCSEL. Moreover, a threshold current of 0.8 mA was achieved. The curvature radius of the micro-lens can be optimized further to extend the area size encircled by the first minimum reflectivity ring and make the micro-lens integrated VCSEL maintain single-mode operation throughout the applied current injection.

Funding. National Key Research and Development Program of China (2017YFB0503200); National Natural Science Foundation of China (NSFC) (11674314, 11774343, 61434005, 61474118, 61727822); Science and Technology Program of Jilin province (20160203013GX); Youth Innovation Promotion Association of the Chinese Academy of Sciences (2017260); Science and Technology Program of Changchun, China (15SS02); Chinese Academy of Sciences (CAS) President's International Fellowship Initiative (2018VTA0005).

REFERENCES

1. H. J. Unold, M. Grabherr, F. Eberhard, F. Mederer, R. Jager, M. Riedl, and K. J. Ebeling, "Increased-area oxidised single-fundamental mode VCSEL with self-aligned shallow etched surface relief," Electron. Lett. **35**, 1340–1341 (1999).
2. C. Carlsson, C. A. Barrios, E. R. Messmer, and A. Lovqvist, "Performance characteristics of buried heterostructure VCSELs using semi-insulating GaInP:Fe regrowth," IEEE J. Quantum Electron. **37**, 945–950 (2001).
3. Y. Ohiso, H. Okamoto, R. Iga, K. Kishi, and C. Amano, "Single transverse mode operation of 1.55 μm buried heterostructure vertical-cavity surface-emitting lasers," IEEE Photon. Technol. Lett. **14**, 738–740 (2002).
4. K. L. Lear, R. P. Schneider, K. D. Choquette, and S. P. Kilcoyne, "Vertical cavity surface emitting lasers with 21% efficiency by metalorganic vapor phase epitaxy, " IEEE Photon. Technol. Lett. **6**, 1053–1055 (1994).
5. C. J. Chang-Hasnain, M. Orenstein, A. Von Lehmen, and L. T. Florez, "Transverse mode characteristics of vertical cavity surface-emitting lasers," Appl. Phys. Lett. **57**, 218–220 (1990).
6. A. J. Danner, T. S. Kim, and K. D. Choquette, "Single fundamental mode photonic crystal vertical cavity laser with improved output power," Electron. Lett. **41**, 325–326 (2005).
7. D. S. Song, S. H. Kim, H. G. Park, C. K. Kim, and Y. H. Lee, "Single-fundamental-mode photonic-crystal vertical-cavity surface-emitting lasers," Appl. Phys. Lett. **80**, 3901–3903 (2002).
8. I. S. Chung, P. Debernardi, Y. T. Lee, and J. Mørk, "Transverse-mode-selectable microlens vertical-cavity surface-emitting laser," Opt. Express **18**, 4138–4147 (2010).
9. H. T. Hsieh, V. Lin, J. L. Hsieh, and G. D. J. Su, "Design and fabrication of long focal length microlens arrays," Micro Nano Lett. **6**, 523–526 (2011).
10. Y. Fu, "Integration of microdiffractive lens with continuous relief with vertical-cavity surface-emitting lasers using focused ion beam direct milling," IEEE Photon. Technol. Lett. **13**, 424–426 (2002).
11. Q. S. Li, L. J. Wang, Z. N. Tian, X. F. Lin, T. Jiang, J. Zhang, X. Zhang, J.-H. Zhao, A.-W. Li, and L. Qin, "Direct integration of aspherical microlens on vertical-cavity surface emitting laser emitting surface for beam shaping," Opt. Commun. **300**, 269–273 (2013).
12. I. Kardosh, F. Demaria, F. Rinaldi, S. Menzel, and R. Michalzik, "High-power single transverse mode vertical-cavity surface-emitting lasers with monolithically integrated curved dielectric mirrors," IEEE Photon. Technol. Lett. **20**, 2084–2086 (2008).
13. N. A. Maleev, A. G. Kuz Menkov, M. M. Kulagina, Y. M. Zadiranov, A. P. Vasilev, and S. A. Blokhin, "Single-spatial-mode semiconductor VCSELs with a nonplanar upper dielectric DBR," Semiconductors **47**, 993–996 (2013).
14. Ph. Nussbaum, R. Völkel, H. P. Herzig, M. Eisner, and S. Haselbeck, "Design, fabrication and testing of microlens arrays for sensors and microsystems," J. Eur. Opt. Soc. **6**, 617–636 (1997).
15. Z. Wang, Y. Ning, T. Li, J. Cui, Y. Zhang, G. Liu, X. Zhang, L. Qin, Y. Liu, and L. Wang, "High-power large-aperture bottom-emitting 980-nm VCSELs with integrated GaAs microlens," IEEE Photon. Technol. Lett. **21**, 239–241 (2009).
16. Y.-S. Kim, J. Kim, J.-S. Choe, Y.-G. Rob, H. Jeon, and J. C. Woo, "Semiconductor microlenses fabricated by one-step wet etching," IEEE Photon. Technol. Lett. **12**, 507–509 (2000).
17. S. Adachi and K. Oe, "Chemical etching characteristics of (001) GaAs," J. Electrochem. Soc. **130**, 2427–2435 (1983).